ISSN (Print) 1226-1750
ISSN (Online) 2233-6656
Journal of Magnetics 22(4), 539-549 (2017) https://doi.org/10.4283/JMAG.2017.22.4.539

A Study on Finding Optimum Parameters of a Diamagnetically Driven Untethered Microrobot

Anil Demircali, Kadir Erkan, and Huseyin Uvet*

Yildiz Technical University, Department of Mechatronics Engineering, Istanbul, Turkey

(Received 26 May 2017, Received in final form 15 November 2017, Accepted 19 November 2017)

In this study, we present a theoretical and numeric analysis of an untethered microrobot manipulation technique that can be used in a liquid environment. A microrobot, which is levitated on a pyrolytic graphite surface, allows us to achieve high precision positioning (at nano level) and control with lower external magnetic force requirements due to stabilizing manner of its locomotion. Stabilizing microrobot is controlled via a single "lifter magnet" as a driving force that is placed on an automatic micro-stage in order to provide stable-motion about x, y and z axes. The presented microrobot is designed for single cell manipulation and transportation operations in liquid medium. It can be used in different experimental setups such as lab-on-a-chips, petri dishes. Here, a new approach to determine an optimal experimental setup of the diamagnetically levitated microrobot, which provides the most effective and possible microrobot control, is explained with FEM (Finite Element Method) analysis and required background information. For such untethered microrobot control experiments in a FEM program, determination of the size of materials used, selection criteria, required magnetic force effects, and optimum pyrolytic graphite sizes are discussed in detail. To do that, our proposed analysis method suggests how to construct such an FEM model parametrically in COMSOL®. Before starting the experimental work, the effects of the material and dimensions of each element forming the system on the microrobot are discussed in detail. Moreover, the manipulation technique which revealed the theoretical infrastructure is compared with the numerical calculations and the results are shown to be compatible with each other.

Keywords : untethered microrobot, diamagnetic levitation, precise manipulation, FEM analysis

1. Introduction

Untethered manipulation and magnetically actuated microrobots are used in mostly biological and medical applications such as cell manipulation, drug delivery, diagnostics, biosensing, chemical synthesis, biopsy, microparticle transport, etc. where minimal damage to the working area is desired [1-6]. Many examples of microrobot have recently been developed for *in vitro* applications including helical swimmers, microgrippers, and soft microparticles [7-9]. In the liquid environments, their fields of application are especially in biomedical engineering for better micro object manipulation without physical linkage or connections [10-12]. When the effect of liquid conditions are taken into account, these methods provide better characteristics in terms of the required magnetic forces and the precision of motion [2].

In the process of designing micro size robots, it will be realized that due to the diminishing dimensions, the flow regime of the liquid environment may change. At this level, the fact that the environment exhibits laminar flow characterization means that the Re (Reynolds Number) is a significant factor. Arai and his team investigated the effects of Reynolds number on microrobot size reduction in a microfluidic environment [13]. Nelson and his team have worked on "sub-mm sized untethered microrobot inside body fluids with external magnetic fields". In addition to the Reynolds effects, the team described the drag force effects in the microfluidics during the movement of the robot [14]. Moreover, Nelson and his team have performed precise position control with three electromagnets. In the work they produce by the inspiration of bacterial manipulation, they have observed drag force and Low-Reynolds effects [7]. Metin Sitti and his team also achieved microrobot control in a contactless manner. During the experiments, errors in movement accuracy

*Corresponding author: Tel: +90-533-385-3023
Fax: +90-212-383-2975, e-mail: huvet@yildiz.edu.tr

were observed. These errors are due to the experimental uncertainty in the measured values of the friction coefficients and the adhesive force [15]. Khamesee and his team have done a precise position control by using a model of the frictional force on the microrobot [16]. However, there are problems with control sensitivity due to frictional force with the surface of the microrobot. Arai and his team have achieved successful results by applying ultrasonic vibrations on the working surface of the microrobot [17, 21, 22]. In these studies, the ultrasonic waves applied to the surface reduce the friction force and increase the end-effector positioning accuracy of a microrobot. This allows them to achieve a movement accuracy of a few microns. Even though, this improved method is a successful example for the "oocyte enucleation" method, it causes cell-immobilization problems in cells and objects that are smaller than the oocyte cell (about 100 μm). This is due to the induced ultrasonic waves in the medium, which causes the objects in the medium to displace. Pelrine and his team have worked on microrobot swarm structures using diamagnetic levitation [18], but for a single microrobot large electromagnets or four permanent magnets are used. Because the study was not done in a fluidic environment, the viscous effects of the fluid were not observed. In our study, diamagnetic levitation is applied to the microrobot in the fluid and two permanent magnets are used as stabilizer and lifter respectively. In this regard, the new manipulation technique applied contributes to the literature.

The aim of the proposed new method is to improve the microrobot manipulation technique, which can be driven in a liquid with high accuracy by detaching microrobots relation from the bottom surface of the liquid medium container. No huge electromagnets or large permanent magnets are needed as because of the fact that the friction force between the bottom surface of the container and microrobot is removed. By using pyrolytic graphite and taking advantage of the diamagnetic forces, the microrobot can have more stable motion characteristic. Thus, nano-accurate manipulations can be performed and a precise control can be achieved.

For achieving a motion accuracy of nanometers, drag forces must be taken into account [7, 14]. The drag force coefficient expressions may be seen in formulas that can be simplified in the corresponding axis when the geometric structure is spherical, disk-shaped, etc., [7, 14, 15, 19]. However, the proposed solutions and analysis techniques are not applicable to different geometries or more complex geometric structures. For this reason, our solution for calculating the drag forces on the structures with complex geometry is to use CFD (Computational Fluid Dynamics) analysis. Motion characteristics, along with the possible movements on the X-Y-Z axes, have been demonstrated with 6-axis control analyzes by applying different scenarios. All cases were handled separately in the analyzes and the changes on the microrobot motion were given.

2. Size Estimation of Materials to be Used-Mesh Effects-Test Setup

The precise calculation of the magnetic forces acting on a microrobot is necessary to its levitation characteristics. This calculation can be done either theoretically, experimentally or numerically (using FEM). The FEM analysis tool that we have used (COMSOL® ver 5.3), has the advantage of being easily applicable to different scenarios. The reason for which COMSOL® was preferred is that it allows multiple physics problems to be combined and parametrically resolved in a single analysis. It also has strong post-processing tools that allow the presentation of the resulting data in a clear manner. For this reason, the COMSOL® tool was preferred for the calculation of the drag force during levitation. Since the geometric structure of the microrobot is rather complex, there are no simple mathematical expressions that we can use, as opposed to cylindrical of spherical structures. For the case at hand, FEM simulations were necessary, because the parameters couldn't be calculated theoretically or through some simple formulas. For this reason, the "drag force" on the microrobot which does not have a simplified or linearized

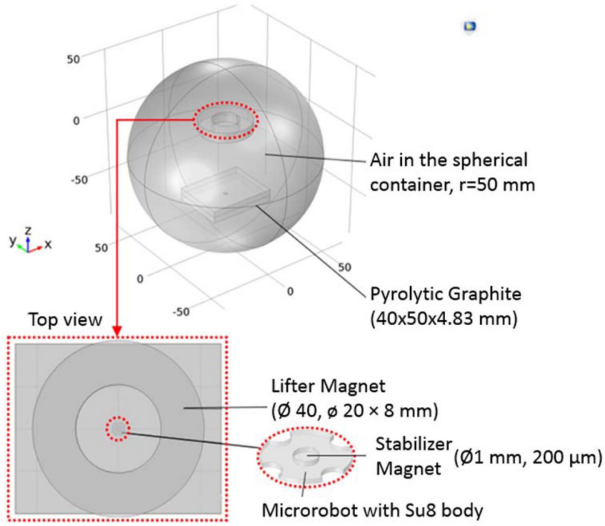

Fig. 1. (Color online) Materials and dimensions used in the experimental setup are shown. Ring type lifter magnet, microrobot and its permanent magnet are aligned to the center of the lifter magnet while pyrolytic graphite is placed on the bottom surface.

mathematical equation, was calculated using COMSOL®. Prior to the FEM analysis, choosing the right materials and correct dimensions are crucial. The entire experimental setup used in the FEM analysis is shown in Fig. 1. In the experimental setup we have built, which was to be modelled in the COMSOL® environment, we used a liquid medium of DI water. A diamagnetic pyrolytic graphite was placed on the bottom surface of the DI water container. On the graphite surface, the SU-8 polymer-based microrobot with a permanent N-52 grade magnet at its center was placed. The lifter magnet was selected as a ring type magnet to be able to utilize laser or vision sensors to get position feedback from the robot in the future. The lifter magnet was positioned above the z-axis of the container.

After selection of the materials for each simulation object, the microrobot was designed according to target application area e.g. cell manipulation, diagnostic etc. Thus, in this study we designed the microrobot, which is shown in Fig. 2, with four carrier slots for effective cell transfer. Because of the its symmetrical nature, it can be more suitable for cell transfer applications. A permanent magnet with a diameter of 1 mm, and a thickness of 0.2 mm was placed at center of the microrobot, which has an outer diameter of 3 mm, to maintain desired levitation.

For a microrobot, whose dimensions are held constant, sizes of the lifter magnet and the pyrolytic graphite used are important because, due to their size effects, the magnetic and diamagnetic forces exerted on the microrobot may change. Before starting to model the experimental setup in COMSOL®, the dimensions of the lifter magnet and the pyrolytic graphite should be defined. In our work, different size magnets were analyzed using parametric analysis methods so as to compare the effects of different dimension magnets on the microrobot. The region where the magnetic forces are linear was selected to achieve

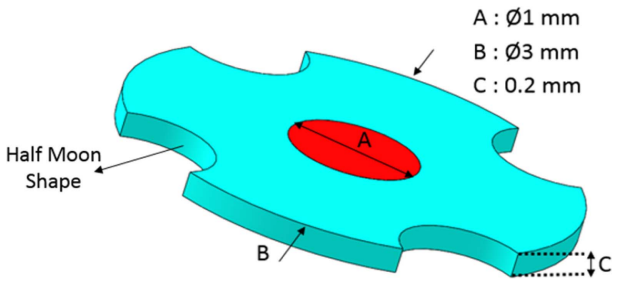

Fig. 2. (Color online) The stabilizer magnet (A) has properties of neodymium (N52 grade) with 1.43 [T]. To transport living cells in a liquid environment, the microrobot has a symmetrical 4 half-moon shape (r: 0.5 mm) carrier slots and 1 central magnet hole for the stabilizer magnet. The SU-8 polymer used as microrobot material, which is well suited for future nano-fabrication process, has a thickness of 200 μm.

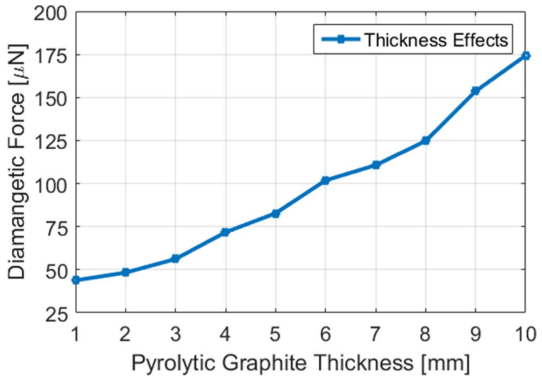

Fig. 3. (Color online) The effect of pyrolytic graphite thickness varying in 1-10 mm on diamagnetic force was calculated. Since the diamagnetic force behaves more linearly in the range of 3-7 mm, material thickness in this range can be selected to get better levitation performance.

more stable levitation characteristics. We chose 5 mm thickness of the pyrolytic graphite since 3-7 mm thickness range had a better linear force performance as shown in Fig. 3. Moreover, as seen in Fig. 3 again, even though there is a 10-fold increase of thickness in the 1-10 mm range, the diamagnetic force increases only about 4 times. Thus, it can be seen that the thickness of the pyrolytic graphite is not proportional to the diamagnetic force generated. The thickness effect could be eliminated by selection of the lifter magnet size to increase/decrease the levitation force.

Microrobot consists of two materials; SU-8 body and central stabilizer magnet as shown in Fig. 2. The diamagnetic force, that is used for achieving stable and planar levitation, applies only on the stabilizer magnet. For calculation of the diamagnetic force on the microrobot, a homogenous material distribution was assumed. Thus, the force per unit volume, dv, on the magnetic field of the microrobot's stabilizer magnet can be expressed as,

$$df = M_d(\nabla B)dv \tag{1}$$

where M_d is the magnetization of the diamagnetic

Table 1. Parameters of Magnetic Forces.

Parameters	Explanation	Unit
B	Magnetic flux density	T
H	Magnetic field strength	A/m
M	Magnetization vector	A/m
χ	Magnetic insulation coefficient	-
μ_r	Relative permeability	-
μ_0	Vacuum permeability	Wb/Am
$n_{x,y,z}$	Surface normal	-

material. Other parameters were given at Table 1 for ease of reading. Since the χ_d value is very small, M_d can be expressed as,

$$M_d = \frac{\chi_d}{\mu_0} B \tag{2}$$

The expression (2) is substituted to (1) and the integral was taken for each axis of the pyrolytic graphite. In this way, the force between the graphite and the stabilizer magnet were calculated as follows:

$$\begin{aligned} F_{\text{dia,x}} &= \frac{\chi_d}{\mu_0} \iiint_V \left(B_x \frac{\partial B_x}{\partial x} + B_y \frac{\partial B_y}{\partial x} + B_z \frac{\partial B_z}{\partial x} \right) dv \\ &= \frac{\chi_d}{2\mu_0} \iiint_V \left(\frac{\partial \|B\|^2}{\partial x} \right) dv \end{aligned} \tag{3}$$

$$\begin{aligned} F_{\text{dia,y}} &= \frac{\chi_d}{\mu_0} \iiint_V \left(B_x \frac{\partial B_x}{\partial y} + B_y \frac{\partial B_y}{\partial y} + B_z \frac{\partial B_z}{\partial y} \right) dv \\ &= \frac{\chi_d}{2\mu_0} \iiint_V \left(\frac{\partial \|B\|^2}{\partial y} \right) dv \end{aligned} \tag{4}$$

$$\begin{aligned} F_{\text{dia,z}} &= \frac{\chi_d}{\mu_0} \iiint_V \left(B_x \frac{\partial B_x}{\partial z} + B_y \frac{\partial B_y}{\partial z} + B_z \frac{\partial B_z}{\partial z} \right) dv \\ &= \frac{\chi_d}{2\mu_0} \iiint_V \left(\frac{\partial \|B\|^2}{\partial z} \right) dv \end{aligned} \tag{5}$$

If the diamagnetic force components on x, y, z axes are simplified according to Ostrogradsky's divergence law [20], $F_{d,x}$, $F_{d,y}$, $F_{d,z}$ can be expressed in surface integral form,

$$F_{\text{dia,x}} = \frac{\chi_d}{\mu_0} \oiint_S \|B\|^2 \, n_x ds \tag{6}$$

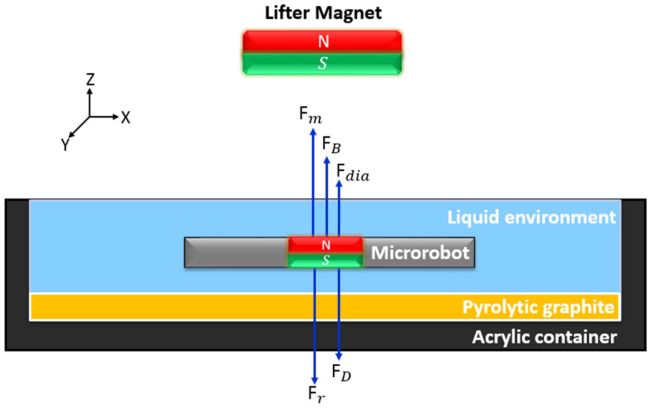

Fig. 4. (Color online) Shows the forces acting on microrobotic arm while it is levitated on a liquid environment. F_m: Lifter magnet force, F_B: Buoyant force, F_{dia}: Diamagnetic force, F_r: Gravitational force, and F_D: Drag Force

$$F_{\text{dia,y}} = \frac{\chi_d}{\mu_0} \oiint_S \|B\|^2 \, n_y ds \tag{7}$$

$$F_{\text{dia,z}} = \frac{\chi_d}{\mu_0} \oiint_S \|B\|^2 \, n_z ds \tag{8}$$

To provide stable levitation of the microrobot, all of the forces acting on it in liquid environment must be determined. Fig. 4 shows the force relations between lifter magnet, microrobot and pyrolytic graphite, when they are placed in an acrylic liquid container.

To find out proper relations between them, COMSOL® MFNC (Magnetic Field No Currents) module for magnetic force analysis, and COMSOL® FSI (Fluid Structure Interface) module for drag force analysis, were performed separately. For the proposed experimental setup shown in Fig. 4, we did not add the liquid container made by acrylic-glass which will be utilized in real experiments. The effect of the acrylic-glass can be ignored since pyrolytic graphite and stabilizer magnet relations are unaffected by the acrylic-glass. Moreover, we choose DI water to create the liquid environment. Independent of the DI water level in it, magnetic effect of the container is the same as the air since both air and DI water have similar relative permeability values. The parameters and their explanations shown in Fig. 4 are given in Table 2.

As can be seen from Fig. 4, F_m, F_{dia} and F_D are variable forces; F_B and F_r are constant forces. For the parametric analysis, the lifter magnet size and its distance to the pyrolytic graphite on the z axis must be calculated. Determining of the lifter magnet force effect on the microrobot in different heights is very important, because it microrobot can be floated in different levels inside the container. When determining this height, the magnetic and non-magnetic forces acting on it microrobot along the z-axis must be taken into account. The height at which the microrobot can float is the point where the sum of these forces are equal to zero. Thus, firstly, the non-magnetic forces are expressed by the equations F_r, F_b and

Table 2. Parametric expressions of forces during levitation and their explanations.

Parameters	Explanation	Unit
m_r	Robot mass	kg
g	Gravitational acceleration	m/s^2
V_r	Robot volume	m^3
ρ_f	Fluid density	kg/m^3
ρ_r	Robot density	kg/m^3
c_d	Drag coefficient	-
A	Cross sectional area	m^2
v	Velocity	m/s

F_d (9-11).

$$F_r = m_r g \tag{9}$$

$$F_B = V_r(\rho_r - \rho_f)g \tag{10}$$

$$F_D = \frac{1}{2} c_d \rho_f A v^2 \tag{11}$$

As can be seen from equation (9), m_r depends on robot mass and can easily be calculated according to the materials used. Since V_r, ρ_r, and ρ_f parameters used in the equation (10) are related to the fluid and microrobot used, no analysis is required in their calculations. However, in (11), the drag coefficient value c_d and F_D which effects on the microrobot during its movement depend on the surface stress force. Hence, FSI analysis was performed firstly to calculate the drag force given in Equation (11). Time-dependent analyses allow the simulation conditions to vary with time. For this reason, instead of "stationary", "time-dependent" analysis method is used in drag force calculation. The movement of the microrobot in the fluid requires overcoming a certain force of inertia. Therefore, the force that must be applied to levitate it microrobot may vary instantaneously. In order to observe this variability and to calculate the time at which the inertia force of the microrobot surpassed, "time-dependent" analysis is performed. The mesh structure that gives the most time effective and precise results for the calculation of c_d parameter in COMSOL® FSI analysis is shown in Fig. 5. Moreover, corner refinement property of COMSOL® can also be used to get more accurate stress values on the corners of the microrobot.

Accordingly, in the relevant analysis shown in Fig. 5,

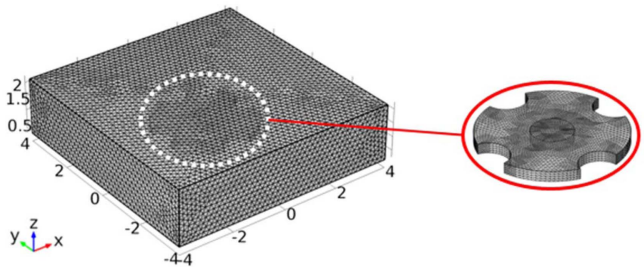

Fig. 5. (Color online) The mesh structure used in FSI analysis is shown. The microrobot is placed in the water-filled container with 4 × 4 × 2 mm outer surface. The effects of different surface stress force, F_D, acting on a microrobot surface are calculated. For a more accurate and precise result, the microrobot has been assigned a minimum width of 0.2 mm, and a thickness of 2 times the thickness of a maximum 0.4 mm mesh. A maximum of 0.5 mm was selected for the container. It is also applied to the system at regular refinement level 2. It can be seen that the mesh-size values should be very close and the direct solver method should be used to have more accurate results.

the c_d value against varying surface stresses and speed of microrobot was also determined. Then, total non-magnetic forces should be found first to calculate necessary magnetic forces, which were generated by pyrolytic graphite and lifter magnet. Surface stress changes on the microrobot and the velocity values at the on its surface are shown in Fig. 6.

The stress values that were obtained from the analysis are used to determine the c_d parameter in equation (11) and the result is shown in Fig. 7.

The calculations are plotted for c_D = 7.6811 in Fig. 7. The c_D value is a constant that can be used for 3 axis

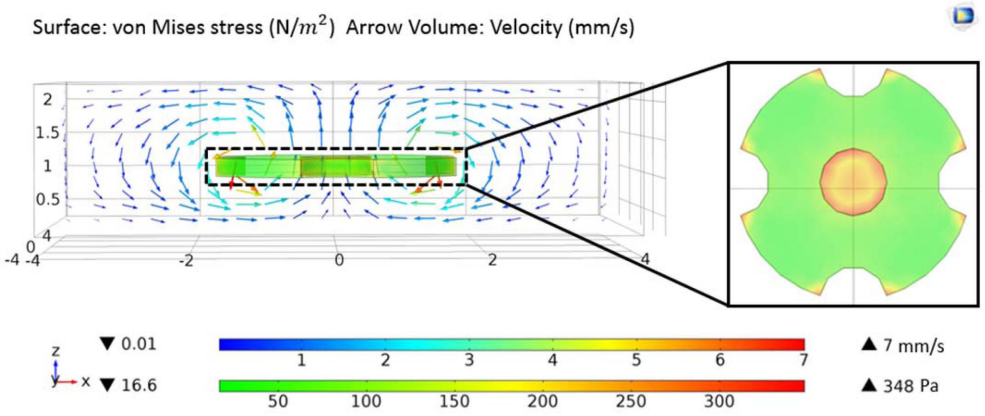

Fig. 6. (Color online) Vector plot of surface stresses on the microrobot is seen for various velocity values. When the velocity of the microrobot is selected 3 mm/s, light blue-green colors were observed more intensively around microrobot and it is given in the upper legend. Surface stress can be seen in the lower legend which is in the range of 16.6-348 Pa. Microrobot body (SU-8) and carrier magnet have different mechanical hardness. Thus, surface stress is seen more intensively at the corner and intersection points between Su-8 & stabilizer magnet. For this reason, the stress in the surface is higher in the intersection regions, while the stress in the magnet center is less and homogeneously distributed.

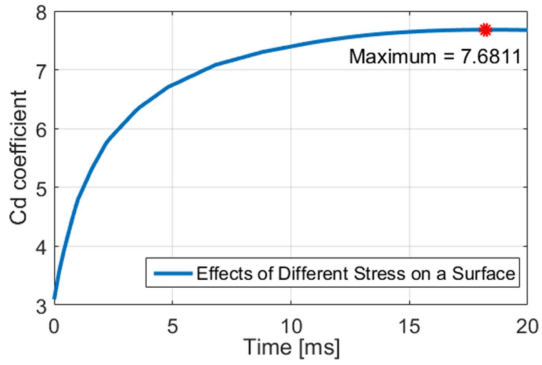

Fig. 7. (Color online) As can be seen, a nearly constant $c_d = 7.6811$ coefficient characteristic is obtained after a certain period of time. F_D can be changed depending on the micro stage speed that we have used. When the microrobot speed is selected as ± 2 mm/s, then F_D is obtained as 0.125 μN. At the same time, it is seen that the value of the drag force that varies parabolically in this range is negligible, because it is about 1/1000 of the diamagnetic force.

movements of the microrobot. According to equation (11), the maximum amplitude of the drag force, which depends on the velocity and cross-sectional area, will occur during levitation. For this reason, during levitation from the z-axis upwards, the drag force on the A_Z cross-sectional area is about 6.6 times greater than A_x as can be seen in Fig. 2. It is seen that the drag force (0.0142mN for speed of 2 mm/s) that can occur in the lateral movements of the microrobot is actually too small to be considered significant. The variation of the drag force on the microrobot at different speed values is shown in Fig. 8. At the beginning, when the microrobot starts moving from the stationary state, there is going to be a drag force. At higher velocities, the drag force change is exponential.

Newton's 1st law of inertia and the dynamic principle of Newton's 2nd law are exposed to a friction and viscous forces on the opposite side of the magnetic forces acting on the microrobot in the x-axis. Besides, during the movement of the "lifter magnet" there is no friction in the air. As a result different accelerations occur in the lifter magnet and microrobot motions. Thus, their parallel movement causes a disruption in the alignment of their centers.

After the determination of the pyrolytic graphite thickness and F_D, the lifter magnet force can be calculated. All magnetic forces are unified to get a single parameter, F_{net}, in the equation (12). F_D force is neglected because it is small. Furthermore, total force, F_T, acting on the microrobot can be obtained by adding together F_B and F_r as in (13).

$$F_{net} = F_m + F_{dia} \tag{12}$$

$$F_T = F_{net} - F_r \tag{13}$$

When $F_T = 0$, it is the condition for levitation is met for a specified gap clearance. F_B, F_r, and F_D are constant forces and they are given in Table 3.

However, to achieve the levitation condition, the net force, F_{net}, to be applied on the microrobot should be

Table 3. Constant Force Values.

Forces	Value	Unit
F_B	12.788	μN
F_r	28.828	μN
F_D	0.125	μN

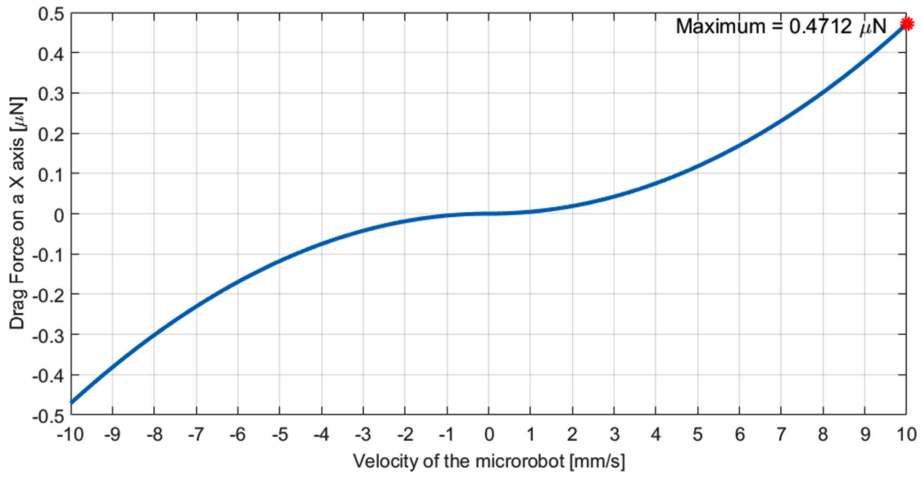

Fig. 8. (Color online) Drag force due to microrobot velocity is shown. This force is the main reason for the misalignment that occurs. This force, which depends on the square of the velocity and is shown in Eq. (11), is obviously not to be neglected, especially at high velocities. For example, a drag force of about 0.1 μN at 5 mm/s is about 0.5 μN when the velocity is 10 mm/s.

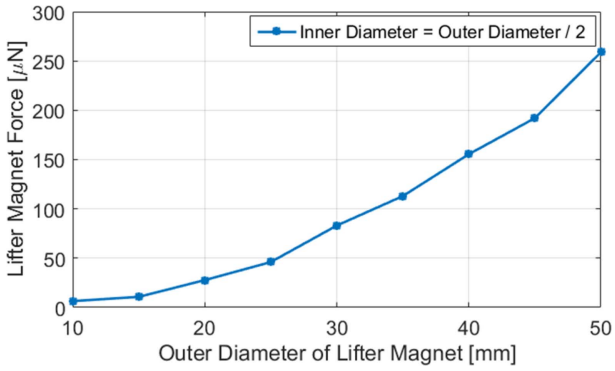

Fig. 9. (Color online) The dimension-effect of the lifter magnet with respect to microrobot is shown. The lifter magnet, which is a more linear force characteristic in the range of 25-45 mm, exhibits exponential behavior according to outside of this range. The selection criterion in this range would be to select a value that is greater than or equal to 2 times the diamagnetic force. It is preferred to use magnets having an outer diameter of 40 mm, an inner diameter of 20 mm and a thickness of 8 mm, which are within the appropriate and acceptable linear range of the relevant value.

around 16.165 μN. The attractive magnetic force, which is applied by the lifter magnet, acting on the microrobot, is expressed in volume and surface integral form

$$F_m = \frac{\mu_r - 1}{2\mu_0\mu_r} \iiint_V \nabla B^2 dv \tag{14}$$

$$F_m = \frac{\mu_r - 1}{2\mu_0\mu_r} \iint_S B^2 ds \tag{15}$$

Equation (14) indicates that a magnetic field gradient needs to be generated on the microrobot. Hence, the position of the microrobot can be controlled by positioning the gradient of the magnetic field within it, relative to the

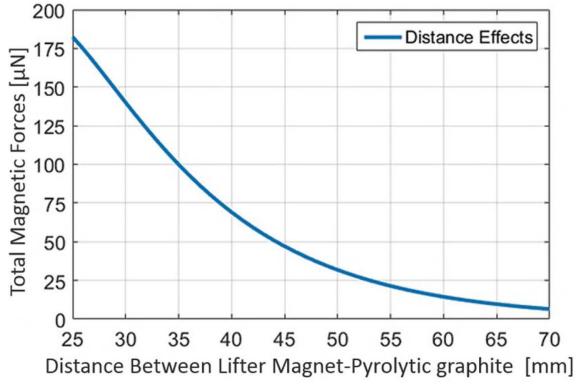

Fig. 10. (Color online) According to our calculations, we found that total magnetic force (F_{net}) on microrobot should be around 16.165 μN for stable levitation. Thus, optimum distance between lifter magnet and pyrolytic graphite may be varied in the range of 52 mm to 64 mm.

microrobot. The size of the lifter magnet was determined according to the diamagnetic force generated by pyrolytic graphite which has a specific thickness (5 mm). The ring shape of magnet is selected as the lifter magnet (for future experimental work) that is shown in Fig. 9. The ratio of inner diameter to outer diameter is 1/2.

As a result of the analysis so far, a graph of the net force generated on the z-axis of microrobot against the distance between the pyrolytic graphite and the lifter magnet is shown in Fig. 10.

3. Determination of Levitation Characteristic, Planar Stable Motion, Misalignment, Head Tilt Analyses

In the previous section, each one of the forces that effect the levitation of microrobot have been analyzed and design parameters were determined individually. This section presents the integration of the experimental COMSOL setup and investigates the interrelation of each component in the following order:

- The effect of net magnetic force that is dependent on the distance between lifter magnet and pyrolytic graphite,
- The effect of misalignment of the robot (whether or not it is aligned to the center of the lifter magnet) on the total force applied to it,
- When the microrobot is tilted rather than parallel to the pyrolytic graphite surface,
- Lifter magnet orientation to correct non-parallel microrobot.

3.1. Levitation Characteristic

In all analyzes, the N-S-N-S representation of the stabilizer magnet and lifter magnet poles are taken as in Fig. 11, the figure also shows the magnetic flux density over the robot and the magnet. The mathematical model of the microrobot in x, y and z axes are expressed as in (16-18).

$$\ddot{x} = \frac{1}{2m_r} c_d \rho_f A_x v_x |v_x| + \frac{(F_{m,x} + F_{g,x})}{m_r} \tag{16}$$

$$\ddot{y} = \frac{1}{2m_r} c_d \rho_f A_y v_y |v_y| + \frac{(F_{m,y} + F_{g,y})}{m_r} \tag{17}$$

$$\ddot{z} = \frac{1}{2m_r} c_d \rho_f A_z v_z |v_z| + \frac{V_r g}{m_r}(\rho_r - \rho_f) - g + \frac{(F_{m,z} + F_{g,z})}{m_r} \tag{18}$$

The F_{net} parameter was determined according to Fig. 10. This force represent the dependence of the total force on the microrobot to different lifter magnet heights. Since the F_{net} value required for levitation is calculated and found in Section 2, the interval at which the microrobot

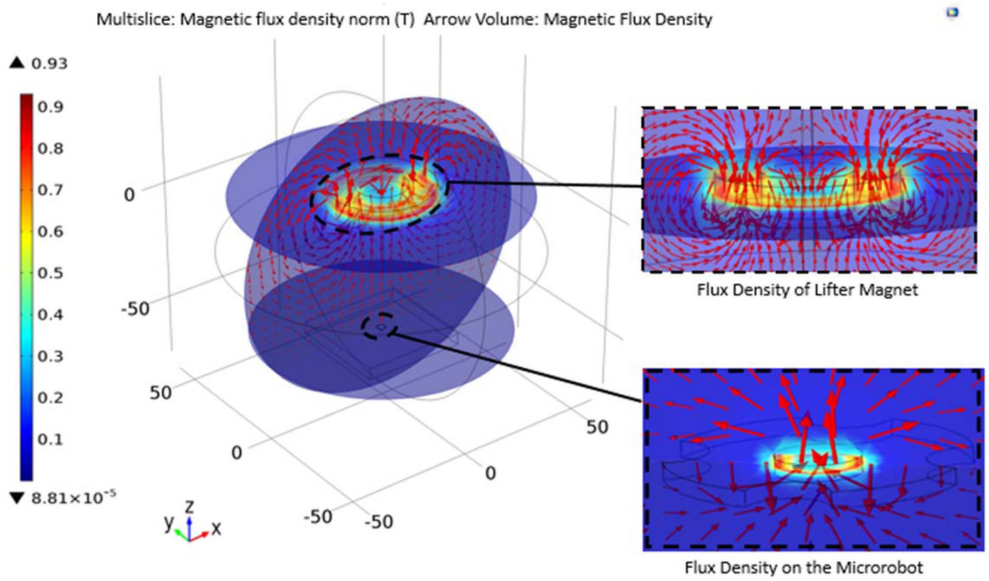

Fig. 11. (Color online) The effect of microrobot levitation height and lifter magnet distance from pyrolytic graphite surface is calculated to find out net magnetic force. The flux density is shown by the Tesla [T] unit with the legend on the left side. The distributions of the flux density in the lifter magnet and stabilizer magnet are given in magnified scale on the right side of the figure. The density is in the range of 0.7-0.9 T in the corners and middle region. The force lines are frequent in that region because of being denser in the corner areas. Since the magnet poles are placed in N-S-N-S, it is shown that the corresponding force (attractive) lines are upwards in the z-axis.

can be levitated is shown in the graph in Fig. 12. This graph shows the effect of total magnetic force at different levitation heights. The optimum working height information of the lifter magnet can be determined by the given legend. The most stable working range is determined to be between 51 m and 306 mm since it has a linear characteristic at this region.

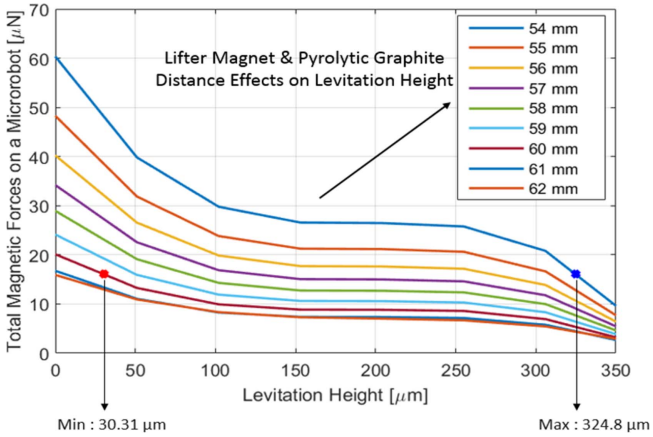

Fig. 12. (Color online) Levitation height of the microrobot is varied depending on lifter-magnet height relative to pyrolytic graphite (optimum range: 54 and 62 mm). Total magnetic force (F_{net}) is ploted to present levitation heights when the lifter magnet is located with 1 mm intervals. A parabolic characteristic of F_{net} can be observed in the figure. Here, microrobot stable levitation range can be found on the graph as between 51 mm and 306 mm due to present more linear behavior.

Also, in Fig. 12, the red point indicates the height at which the microrobot can be levitated and the blue point is the maximum levitation height (detachment point). When these points are chosen, the F_{net} value can be calculated from equation (12) as 16.165 μN. The F_{net} value indicates the total magnetic force required for levitation, which varies with the height of the "lifter magnet".

3.2. Planar Stable Motion and Head Tilting Situations

During the movement of the microrobot, there may be cases where the magnetic forces acting on its surface do not act homogeneously and consequently there is an axial misalignment. This causes the lifter magnet not to be in the same center with the microrobot's stabilizer magnet. In this case, the magnetic field force lines can't be perpendicular to each other due to the head-tilting reaction of the microrobot. This creates an undesired torque on the microrobot perpendicular to pyrolytic graphite. Therefore, the microrobot will not be able to move parallel to the pyrolytic graphite. This means that a locomotion with head-tilting can be considered as a characteristic movement for this study. The head-tilting can be seen only if the lifter magnet moves parallel to the pyrolytic graphite surface. However, when the lifter magnet is rotated relative to the stabilizer magnet, axial misalignment may

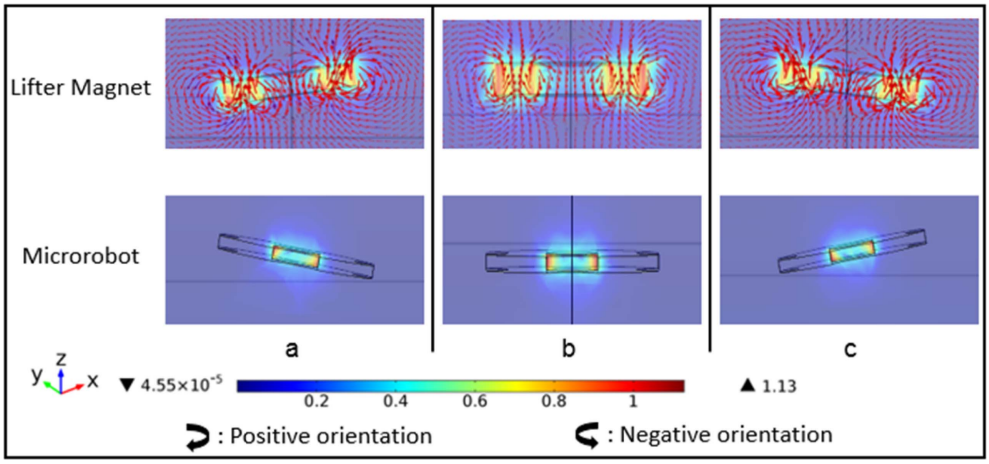

Fig. 13. (Color online) For microrobot's three different motion characteristics, three different orientations of the lifter magnet are shown to avoid undesired torque. All these three combinations are calculated parametrically. As a result, an inverted orientation lifter magnet should be applied according to the orientation of microrobot.

be decreased by providing more homogenous distribution of magnetic force vectors on the stabilizer magnet surfaces. The corresponding head-tilting reactions with respect to different the lifter magnet orientations are given in Fig. 13. As can be seen, the flux density is increased in the edge direction where the lifter magnet bends and the force lines become more intense. As expected, the force lines Fig. 13(a) and 13(c) are not symmetrical compared to Fig. 13(b). Using these properties, undesired torque may be eliminated by giving a negative orientation to the lifter magnet relative to the microrobot.

In this analysis, the head-tilting motion of the microrobot was analyzed for different angles in the range of ± 10°, as can be seen in the Fig. 14. Here, as an example, when the microrobot performs an 8° positive angular orientation, undesired torque that will be induced is calculated. Then, the angle value to which the lifter magnet should be rotated is calculated to prevent undesired torque. This indicated that the lifter magnet must be rotated at an angle opposite to the microrobot slope angle. The aim of the relevant analysis is to ensure that the microrobot moves parallel to the pyrolytic graphite surface. Since microrobot has a symmetrical design, torques generated on x and y axes must be equal, so that only the analysis in x axis is shown.

As a result of the relevant analyses,

1. The best effective working range of lifter magnet is determined as 56-58 mm.

2. The microrobot's levitation height and detachment points are obtained from Fig. 11. Accordingly, stable levitation height has been found in the range of 51-306 μm and detachment points is 324.8 μm.

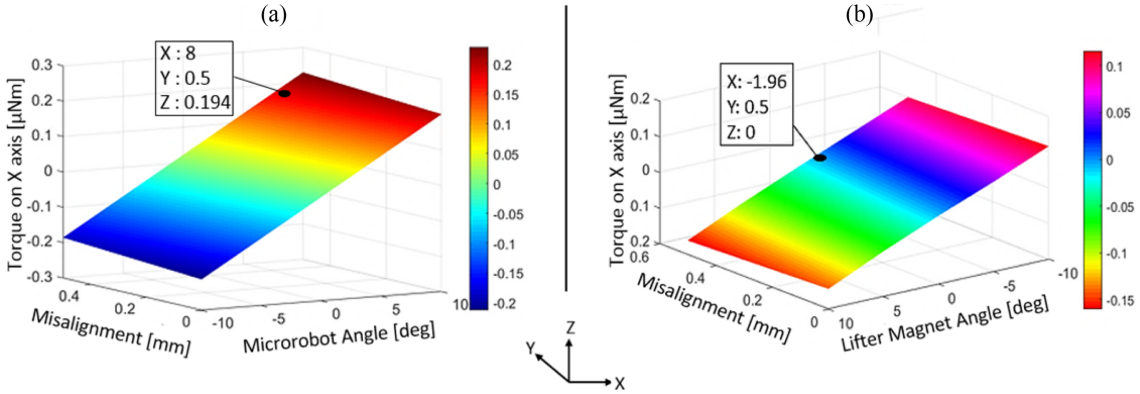

Fig. 14. (Color online) (a) Refers to the orientation case with misalignment of microrobot as a surface graph with linear characteristic. (b) refers to the values of the lifter magnet angles to provide the prevention of undesired torque (0 approach). Graph (a) shows the orientation and misalignment of the resultant undesired torque, which can be prevented by the angle of the lifter magnet in graph (b). In this analysis, it can be seen that −1.96º negative rotation of the lifter magnet is required to obtain 0 mNm torque on x axis when a 0.5 mm misalignment and 8° positive orientation are observed on the microrobot.

3. Head-tilting motion of the microrobot can be controlled by the lifter magnet angular motion.

4. The orientation effects of the lifter magnets are calculated and it is shown that non-parallel motion of microrobot in the range of ± 10° can be controlled by controlling the angular position of the lifter magnet. For example, for the lifter magnet to compensate a +8° tilting of the microrobot, it should be rotated to −1.96°.

By discussing all possible situations given above, the applicability of the relevant design has been demonstrated.

4. Experimental Results

In the previous chapters, the factors that need to be taken into consideration when setting up a microrobot's experimental setup that is based on the principle of diamagnetic levitation. In addition, its microrobot levitation has been shown to be possible, with optimal parameter values selected as the results of the analyses. In this section, first preliminary experiments of the microrobot which was designed and manufactured by the results of analysis that was presented in the previous sections. The experimental system that was set up according to the selected parameters is shown in Fig. 15(a). Preliminary experimental results have shown that the microrobot levitation can be performed using calculated parameters. For the orientation of the lifter magnet, a high precision micro-nano stage (PI M-126.PD2) was equipped and a container with thick pyrolytic graphite is placed right under it. A camera system attached to a microscope lens (Olympus SZX-7 and PointGrey GS3-U3) is utilized for the confirmation of the levitation.

Precise positioning of the lifter-magnet in the z-axis relative to the pyrolytic graphite was achieved by using the micro-nano stage. The results of the analyses were tested to see whether the robot was levitated at the calculated range of 54 mm-62 mm. Firstly, the microrobot which has a higher density than DI water is allowed to sink to the graphite surface. It was observed that by bringing the lifter-magnet to the proper position the mechanical contact of the microrobot from the graphite surface was cut off and the microrobot was suspended in the water. The results of this experiment are shown in Fig. 15, where the confirmation of the micro levitation can be seen in (b), (c) and (d). As shown in the figure and analysis, the microrobot height change can be estimated according to the position of the lifter magnet.

5. Discussion Conclusion

Reliable combination of different physics modules of COMSOL depends heavily on proper mesh generation. The errors that may arise during simulations can be eliminated successfully via proposed methodologies, formulations and calculation techniques. During a COMSOL analyses, it can be the case that large differences and error values can occur in the results depending on the generated mesh. For this reason, the most accurate results can be

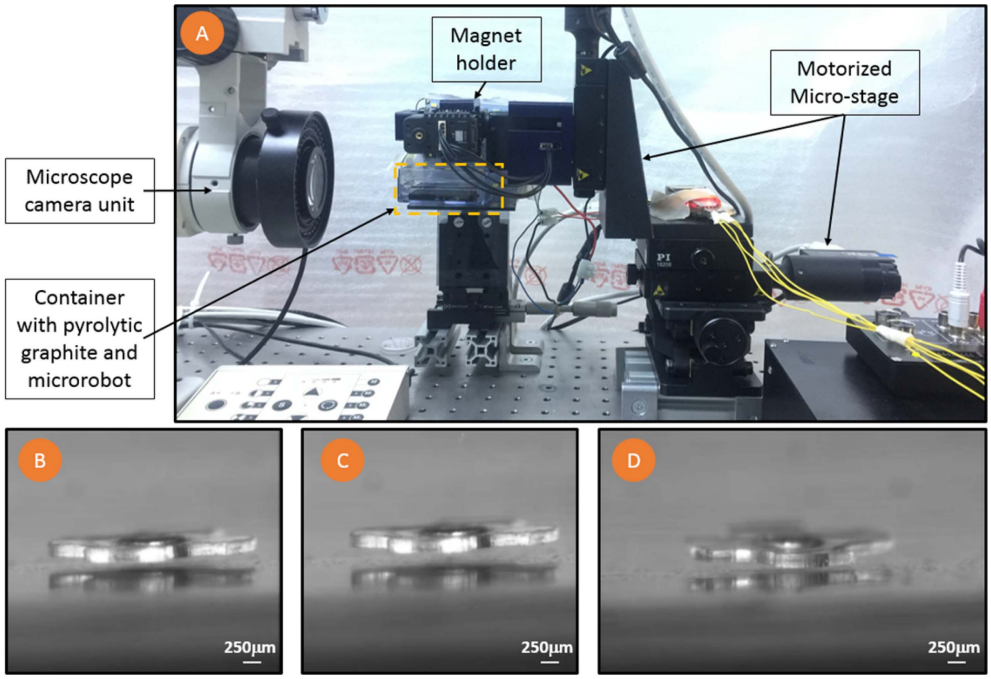

Fig. 15. (Color online) Schematics of the experimental setup.

obtained by experimenting with different meshing methods. For example, for an FSI analysis the minimum and maximum values of tetrahedral meshes should be close to each other. For this reason, "regular refinement level 2" and "corner refinement" have been applied. This resulted in more accurate results in particular for the stress values at corners. Therefore, on the resulting c_d graph, "drag force coefficient" can be calculated by obtaining a smooth exponential graph.

In the MFNC, pyrolytic graphite thickness determination analysis, "mapping mesh" is applied to the upper surface and propagated to the whole component by the "swept" method. By applying "convert-insert center points" option entirely to graphite, graphs with increasing characteristics in response to their thickness values have been obtained. Moreover, in the MFNC lifter magnet sizing analysis, the "free triangular" mesh structure was applied to the surface and then "swept" to the entire component. From the COMSOL "distributions menu", a symmetrical mesh structure is given to the component by adjusting the number of generated meshes based on the selected edge. Thus, the expected graphical characteristics were taken so that experimental setup of the simulation was established.

Acknowledgement

This project with Project No: 113E584 is supported by The Scientific and Technological Research Council of Turkey (TUBITAK).

References

[1] Fusco, S., Sakar, M. S., Kennedy, S., Peters, C., Bottani, R., Starsich, F., and Mooney, D. Adv. Mater. **26**, 952 (2014).
[2] Squires, T. M. and Quake, S. R. Rev. Mod. Phys. **77**, 977 (2005).
[3] Hagiwara, M., Kawahara, T., Yamanishi, Y., and Arai, F. Appl. Phys. Lett. **97**, 013701 (2010).
[4] Zhang, T., Zhang, M., and Cui, T. In Solid-State Sensors, Actuators and Microsystems Conference (TRANSDUCERS), 2011 16th International. IEEE. (2011) pp 306-309.
[5] Nelson, B. J., Kaliakatsos, I. K., and Abbott, J. J. Annu. Rev. Biomed. Eng. **12**, 55 (2010).
[6] Feng, L., Ichikawa, A., Arai, F., and Hagiwara, M. In Manipulation, Manufacturing and Measurement on the Nanoscale (3M-NANO), 2012 International Conference on. IEEE. (2012) pp 59-64.
[7] Zhang, L., Abbott, J. J., Dong, L., Kratochvil, B. E., Bell, D., and Nelson, B. J. Appl. Phys. Lett. **94**, 064107 (2009).
[8] Gultepe, E., Randhawa, J. S., Kadam, S., Yamanaka, S., Selaru, F. M., Shin, E. J., and Gracias, D. H. Adv. Mater. **25**, 514 (2013).
[9] Tabatabaei, S. N., Lapointe, J., and Martel, S. Adv. Robot. **25**, 1049 (2011).
[10] Zhao, X., Kim, J., Cezar, C. A., Huebsch, N., Lee, K., Bouhadir, K., and Mooney, D. J. Proceedings of the National Academy of Sciences **108**, 67 (2011).
[11] Zhang, X. Z., Lewis, P. J., and Chu, C. C. Biomaterials **26**, 3299 (2005).
[12] Ichikawa, A., Arai, F., Yoshikawa, K., Uchida, T., and Fukuda, T. Appl. Phys. Lett. **87**, 191108 (2005).
[13] Fukuda, T., Kawamoto, A., Arai, F., and Matsuura, H. In Micro Electro Mechanical Systems, 1994, MEMS'94, Proceedings, IEEE Workshop on. IEEE. (1994) pp 273-278.
[14] Yesin, K. B., Vollmers, K., and Nelson, B. J. Int. J. Rob. Res. **25**, 527 (2006).
[15] Pawashe, C., Floyd, S., and Sitti, M. Int. J. Rob. Res. **28**, 1077 (2009).
[16] Hosseini, S., Mehrtash, M., and Khamesee, M. B. Microsyst. Technol. **17**, 1145 (2011).
[17] Hagiwara, M., Kawahara, T., Yamanishi, Y., Masuda, T., Feng, L., and Arai, F. Lab on a Chip **11**, 2049 (2011).
[18] Pelrine, R., Wong-Foy, A., McCoy, B., Holeman, D., Mahoney, R., Myers, G., and Low, T. In Robotics and Automation (ICRA), 2012 IEEE International Conference on. IEEE. (2012) pp 739-744.
[19] Peyer, K. E., Zhang, L., and Nelson, B. J. Nanoscale **5**, 1259 (2013).
[20] Katz, V. J. Mathematics Magazine **52**, 146 (1979).
[21] Feng, L., Di, P., and Arai, F. Int. J. Rob. Res. **35**, 1445 (2016).
[22] Feng, L., Hagiwara, M., Ichikawa, A., and Arai, F. Micromachines **4**, 272 (2013).